Available online at www.eccomasproceedia.org
Eccomas Proceedia EUROGEN (2021) 56-69

ECCOMAS
Proceedia

EUROGEN 2021
14th ECCOMAS Thematic Conference on
Evolutionary and Deterministic Methods for Design, Optimization and Control
N. Gauger, K. Giannakoglou, M. Papadrakakis, J. Periaux (eds.)
Streamed from Athens, Greece, 28–30 June 2021

OPTIMIZATION OF A MIXING DEVICE WITH BAFFLES USING THE ENHANCED SURFACE INTEGRAL (E-SI) CONTINUOUS ADJOINT METHOD FOR TWO-PHASE FLOWS

N. Galanos[1], E.M. Papoutsis-Kiachagias[1], and K.C. Giannakoglou[1]

[1]National Technical University of Athens,
Parallel CFD & Optimization Unit, School of Mechanical Engineering
Zografou Campus, 9 Iroon Polytechniou Str
e-mail: galanosn0@gmail.com,{vpapout,kgianna}@mail.ntua.gr

Abstract. *The optimization of a static mixing device, equipped with baffles to enhance mixing, is presented. The tubular device includes a fixed number of equidistant baffles and performs the mixing of two miscible fluids. The optimization aims at redesigning the shape of the baffles by considering two objectives: (a) mixture uniformity at the outlet and (b) total pressure losses inside the device, both depending on the baffles' shapes. To parameterize these shapes, a volumetric B-Splines morphing technique is utilized, adapting the neighboring grid nodes at the same time. The front of non-dominated optimal solutions in the two-objective space is computed by optimizing different weighted sums of the two objective functions. For the computation of their gradients, the continuous adjoint method is mathematically formulated, programmed in OpenFOAM© and used. Compared to previous works by the same research group on the design of similar mixing devices, the so-called Enhanced Surface Integral (E-SI) continuous adjoint method is herein developed and used. This computes sensitivity derivatives based exclusively on surface integrals of the primal and adjoint variables, while considering the effect of grid sensitivities through the formulation and numerical solution of the system of the adjoint to a Laplacian grid displacement model. The E-SI adjoint has been developed in the past for single-phase flows and is extended herein to two-phase flow problems.*

Keywords: Two-Phase Flows, Shape Optimization, Continuous Adjoint Method, Grid Sensitivities.

Peer-review under responsibility of the organizing committee of EUROGEN 2021.
doi: 10.7712/140121.7950.18375

1 Introduction

In fluid mechanics, Computational Fluid Dynamics (CFD) codes along with optimization algorithms can be used to design optimally performing devices. In gradient-based optimization, the derivatives of the objective function with respect to (w.r.t.) the design variables (also known as the sensitivity derivatives, SDs) must be computed at the lowest possible cost; to this end, the adjoint method can be used since it has a cost which does not scale with the number of design variables.

This paper focuses exclusively on continuous adjoint and refrains from commenting on discrete adjoint. The continuous adjoint method is well formulated in the literature for single-phase incompressible and compressible flow problems [11, 12], occasionally including the adjoint to turbulence models [3], and has successfully been used to perform shape and topology optimization. Focusing on the application this paper is dealing with, in [1] the continuous adjoint method to a two-phase flow model for miscible fluids was proposed by the same research group; this was used for the shape optimization of mixing devices of the same type as the one designed herein. However, in [1], the development of the adjoint led to SDs being computed without accounting for the effect of the so-called grid sensitivities. Grid sensitivities are the derivatives of the nodal coordinates of the computational grid w.r.t. the design variables. Depending on the adjoint formulation, the SDs may include volume integrals of grid sensitivities; this is the Field Integral (FI) adjoint formulation. To get rid of grid sensitivities and field integrals in the SDs, the adjoint to a grid displacement model must be included; this gives rise to the Enhanced Surface Integral (E-SI) continuous adjoint [2] this paper is dealing with. Both FI and E-SI adjoints are equally accurate but the latter is computationally less demanding. A "severed" E-SI adjoint is also in use [12, 13], without solving the adjoint grid displacement equations; this is also the approach followed in [1] and may occasionally compute less accurate SDs [2, 4].

Multiphase flows can be found in many industrial simulations. Several industrial multiphase flow applications include the mixing of two or more distinct phases, which is the interest of this paper too. Mixing can be performed in devices with motionless compartments, known as static mixers. These appear in a variety of industrial processes [6, 7], as an alternative to the use of conventional agitators; in the absence of rotating parts, motionless mixers typically have lower energy consumption and reduced maintenance requirements. They perform the blending of the fluids travelling inside them and, if properly designed, deliver a highly homogeneous mixture at the exit [8]. Mixing of the fluids can be enhanced by motionless parts, such as baffles, which force the flow to recirculate. Apart from delivering a uniform flow at the exit, it is also important to keep total pressure drop inside the device as low as possible, to reduce energy consumption [9].

In view of the above, the optimization of a particular mixing device of cylindrical shape with two inlets, from which the two fluids enter separately, and a single outlet, is presented. Mixing of the two fluids is enhanced by six baffles equi-distributed along the axial direction which affect losses and mixing effectiveness. The optimization aims at re-designing these shapes, starting from a baseline half-circular shape. A volumetric B-Splines morphing technique is used to parameterize the shape of the baffles, by also meeting manufacturability constraints. Two objective functions are used in this paper, namely maximum mixture uniformity at the exit and minimum total pressure losses inside the device. To compute the derivatives of these functions, the continuous adjoint method is formulated, programmed in the open-source CFD toolbox of OpenFOAM©, and used (see an overview of the capabilities of the same optimization software in [5], presented in the same conference). Compared to [1], the Enhanced Surface

Integral (E-SI) adjoint formulation is used, in contrast to the severed approach used there. In the past, the E-SI adjoint has been developed for single-phase flow problems [2] and, in this paper, is extended to two-phase flow problems for the first time in the corresponding literature.

2 Case and Adjoint-Based Shape Optimization Framework

2.1 Starting Geometry of the Mixing Device

The mixing device this paper is dealing with, consists of a main cylindrical part of length equal to $0.7m$ and inner diameter of $0.1m$, two inlets, for the two incoming fluids, and a single outlet; both inlets and the outlet have an inner diameter of $0.05m$. The geometry of the device is shown in fig. 1; inside the device, six baffles are equally distributed along the axial direction at a distance of $0.12m$ from each other, to enhance the mixing of the two phases. In the reference/baseline geometry, these have a semi-circular shape and every baffle is shifted by 180° from the previous one.

2.2 Two-Phase Flow Model - Primal Equations

The two fluids, entering the static mixer, are treated as incompressible, miscible fluids using the Volume of Fluid (VoF) method [17–19] to account for their interaction. For a laminar flow, the continuity and momentum equations for two-phase flows coupled with a convection-diffusion phase transport equation read

$$R^p = -\frac{\partial(\rho v_j)}{\partial x_j} = 0 \tag{1}$$

$$R^v_i = \rho v_j \frac{\partial v_i}{\partial x_j} - \frac{\partial\left(\mu \epsilon_{ij}\right)}{\partial x_j} + \frac{\partial p}{\partial x_i} = 0\,, \qquad i = 1,2,3 \tag{2}$$

$$R^\alpha = v_i \frac{\partial \alpha}{\partial x_i} - \frac{\partial}{\partial x_j}\left(D \frac{\partial \alpha}{\partial x_j}\right) = 0 \tag{3}$$

where v_i are the flow velocity components, p the static pressure and $\epsilon_{ij} = \frac{\partial v_i}{\partial x_j} + \frac{\partial v_j}{\partial x_i}$ the strain tensor. In eq. 3, α denotes the volume fraction of fluid 1 and D stands for the mass diffusion coefficient, similarly to Fick's law of diffusion. Repeated indices imply summation.

The mixture's density ρ and dynamic viscosity μ are both a linear combination of ρ_i and μ_i ($i=1,2$) of the two fluids, i.e.

$$\rho = \alpha\rho_1 + (1-\alpha)\,\rho_2 \tag{4}$$

$$\mu = \alpha\mu_1 + (1-\alpha)\,\mu_2 \tag{5}$$

Dirichlet conditions are imposed on v_i and α at the two inlets (S_I) of the mixer, where $\alpha=1$ at Inlet 1 (inlet of the first fluid) and $\alpha=0$ at Inlet 2 (inlet of the second fluid), along with a zero

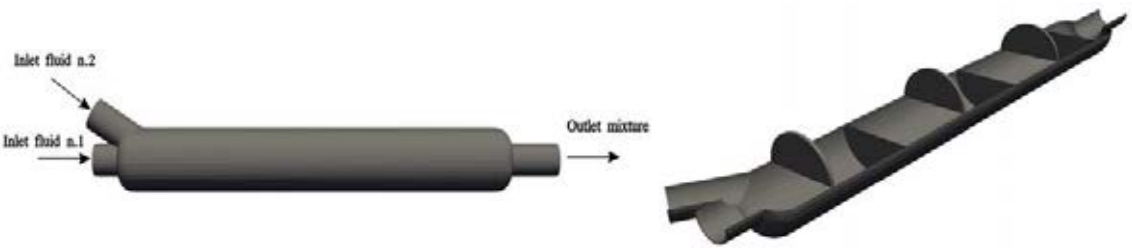

Figure 1: Reference geometry of the static mixing device. Left: a view of the external part, with two inlets, from which two different fluids enter, and a single outlet. Right: perspective view of the six equidistantly placed baffles.

Neumann condition on p. At the single outlet (S_O), zero Neumann conditions are imposed on both v_i and α along with a constant (zero) value for p. Finally, at the solid walls (S_W), a zero Dirichlet (no-slip) condition is imposed on v_i and zero Neumann conditions on p and α.

2.3 Shape Parameterization

A volumetric B-Splines morphing technique is employed to parameterize the shape of the baffles. Let $X_m^{ijk}, m \in [1,3], i \in [0,I], j \in [0,J], k \in [0,K]$ be the value of the $m-th$ coordinate in the cylindrical system of the $ijk-th$ control point in the 3D control grid. These values constitute the design variables of the problem, i.e. the optimization unknowns. The cylindrical coordinates $\mathbf{x} = [r, \theta, z]$ of the grid points residing within the morphing lattice are given by

$$x_m(u,v,w) = U_{i,pu}(u) V_{j,pv}(v) W_{k,pw}(w) X_m^{ijk} \tag{6}$$

where $\mathbf{u} = [u,v,w]$ denotes the grid parametric coordinates. U, V, W are the B-Splines basis functions and pu, pv, pw their corresponding polynomial degree, which may be different per control point direction. A single control lattice parameterizing the shape of a single baffle, as well as the grid points neighboring to the same baffle, is presented in fig. 2.

2.4 The Continuous Adjoint Method

In what follows, b_n,$n \in [1,N]$ is used to denote the design variables. Two objective functions to be minimized, are considered. The first one expresses the volume-averaged mixture uniformity at the outlet of the device, written as

$$J_U = \frac{1}{2} \int_{S_O} v_i n_i (\alpha - \overline{\alpha})^2 dS \ , \quad \overline{\alpha} = \frac{1}{|S_O|} \int_{S_O} \alpha dS \tag{7}$$

where n_i are the components of the unit normal vector pointing outwards of the flow domain and $\overline{\alpha}$ is the mean value of the volume fraction computed at the outlet. The second objective function is the volume-averaged total pressure losses between the inlet(s) and the outlet,

$$J_P = -\int_{S_{I,O}} v_i n_i \left(p + \frac{1}{2} \rho v_j^2 \right) dS \tag{8}$$

The derivatives of the two objective functions w.r.t. the design variables b_n are computed and used to minimize their weighted sum

$$J = w_1 J_U + w_2 J_P \tag{9}$$

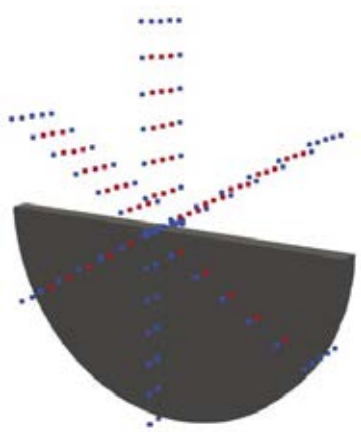

Figure 2: A control grid consisted of 7 points in the radial direction, 7 points in the peripheral direction and 5 points in the mixer's longitudinal direction, used to parameterize the shape of a single baffle. Control points in blue remain fixed during the optimization. Those in red, are active and may change the baffle's shape.

	$\frac{\partial j_{S_i}}{\partial p} n_i$	$\frac{\partial j_{S_k}}{\partial v_i} n_k$	$\frac{\partial j_{S_i}}{\partial \alpha} n_i$
J_U	0	$\frac{1}{2}\left(\alpha-\overline{\alpha}\right)^2 n_k \delta_i^k$	$v_i n_i \left(\alpha-\overline{\alpha}\right)$
J_P	$-v_i n_i$	$-\left(p+\frac{1}{2}\rho v_j^2\right) n_k \delta_i^k - \rho v_k n_k v_i$	$-v_i n_i \frac{1}{2}\rho_\Delta v_j^2$

Table 1: Derivatives of integrands j_{S_i} of the two objective functions w.r.t. the flow variables.

where w_1,w_2 are user-defined weights. By performing a number of single-objective runs with different sets of weights, the front of non-dominated solutions in the objective space can be computed. To facilitate the development of the adjoint, J is written in the form of two surface integrals along S_I and S_O, as follows

$$J = \int_{S_I} j_{S_{I,i}} n_i dS + \int_{S_O} j_{S_{O,i}} n_i dS \tag{10}$$

Using $\frac{\delta \Phi}{\delta b_n} = \frac{\partial \Phi}{\partial b_n} + \frac{\partial \Phi}{\partial x_k}\frac{\delta x_k}{\delta b_n}$ to link the total derivative $\frac{\delta}{\delta b_n}$ of any flow quantity Φ w.r.t. b_n, the partial derivative $\frac{\partial}{\partial b_n}$ and grid sensitivities $\frac{\delta x_k}{\delta b_n}$, the differentiation of eq. 10 w.r.t. b_n gives

$$\frac{\delta J}{\delta b_n} = \int_{S_{I,O}} \frac{\partial j_{S_i}}{\partial b_n} n_i dS + \int_{S_{I,O}} \frac{\partial j_{S_i}}{\partial x_k}\frac{\delta x_k}{\delta b_n} n_i dS + \int_{S_{I,O}} j_{S_i} \frac{\delta \left(n_i dS\right)}{\delta b_n} \tag{11}$$

where (see, also, table 1)

$$\frac{\partial j_{S_i}}{\partial b_n} n_i = \frac{\partial j_{S_k}}{\partial v_i}\frac{\partial v_i}{\partial b_n} n_k + \frac{\partial j_{S_i}}{\partial p}\frac{\partial p}{\partial b_n} n_i + \frac{\partial j_{S_i}}{\partial \alpha}\frac{\partial \alpha}{\partial b_n} n_i \tag{12}$$

The development of the E-SI adjoint starts by defining the Lagrangian

$$L = J + \int_\Omega q R^p d\Omega + \int_\Omega u_i R_i^v d\Omega + \int_\Omega \psi R^\alpha d\Omega + \int_\Omega m_i^\alpha R_i^m d\Omega \tag{13}$$

where q is the adjoint pressure, u_i are the components of the adjoint velocity and ψ is the adjoint volume fraction. Apart from integrals including the equations pertaining to the two-phase flow, L also includes grid displacement PDEs to account for variations in the nodal coordinates of the computational grid due to the changes in the design variables. Herein, a Laplace type grid displacement model, as firstly proposed in [2] for single-phase flows, is assumed

$$R_i^m = \frac{\partial^2 m_i}{\partial x_j^2} = 0 \,, \qquad i = 1,2,3 \tag{14}$$

where m_i denote grid nodal displacements and m_i^α their adjoint. The fact that eqs. 14 are included in L does not imply that this model should necessarily be used to displace the internal grid nodes during the optimization. This is just a convenient, though harmless, assumption (see [15]) made during the development of the E-SI adjoint.

Differentiating L w.r.t. b_n gives

$$\begin{aligned}\frac{\delta L}{\delta b_n} \;=\; & \frac{\delta J}{\delta b_n} + \int_\Omega q \frac{\partial R^p}{\partial b_n} d\Omega + \int_\Omega u_i \frac{\partial R_i^v}{\partial b_n} d\Omega + \int_\Omega \psi \frac{\partial R^\alpha}{\partial b_n} d\Omega + \int_\Omega m_i^\alpha \frac{\partial R_i^m}{\partial b_n} d\Omega \\ & + \int_S \left(q R^p + u_i R_i^v + \psi R^\alpha + m_i^\alpha R_i^m\right) \frac{\delta x_k}{\delta b_n} n_k dS\end{aligned} \tag{15}$$

where the last term emerges from the application of the Leibniz integral rule. The rest of the integrals appearing on the r.h.s. of eq. 15 can further be developed using the Gauss divergence theorem and $\frac{\partial}{\partial b_n}\left(\frac{\partial \Phi}{\partial x_j}\right) = \frac{\partial}{\partial x_j}\left(\frac{\partial \Phi}{\partial b_n}\right)$, according to which spatial and partial derivatives w.r.t. b_n permute. The mathematical development of the first three volume integrals can be found in [1]. The last volume integral on the r.h.s. of eq. 15 becomes

$$\int_\Omega m_k^\alpha \frac{\partial R_k^m}{\partial b_n} d\Omega = \int_S m_k^\alpha n_j \frac{\partial}{\partial x_j}\left(\frac{\delta x_k}{\delta b_n}\right) dS - \int_S \frac{\partial m_k^\alpha}{\partial x_j} n_j \frac{\delta x_k}{\delta b_n} dS + \int_\Omega \frac{\partial^2 m_k^\alpha}{\partial x_j^2} \frac{\delta x_k}{\delta b_n} d\Omega \tag{16}$$

2.4.1 Adjoint Equations

To avoid the computation of partial derivatives of p, v_i and α w.r.t. b_n in the interior of the flow domain, their multipliers inside field integrals in (the developed form of) eq. 15 are set to zero, giving rise to the adjoint set of PDEs, which take the following form (being the same in both the E-SI and FI adjoint formulations)

$$R^q = -\frac{\partial u_i}{\partial x_i} = 0 \tag{17}$$

$$R_i^u = \rho u_j \frac{\partial v_j}{\partial x_i} - \frac{\partial(\rho v_j u_i)}{\partial x_j} - \frac{\partial\left(\mu \epsilon_{ij}^\alpha\right)}{\partial x_j} + \rho \frac{\partial q}{\partial x_i} + \psi \frac{\partial \alpha}{\partial x_i} = 0\,, \quad i = 1,2,3 \tag{18}$$

$$R^\psi = -\frac{\partial\left(v_j \psi\right)}{\partial x_j} - \frac{\partial}{\partial x_j}\left(D \frac{\partial \psi}{\partial x_j}\right) + \rho_\Delta \left(v_i \frac{\partial q}{\partial x_i} + u_i v_j \frac{\partial v_i}{\partial x_j}\right) + \mu_\Delta \frac{\partial u_i}{\partial x_j} \epsilon_{ij} = 0 \tag{19}$$

where $\rho_\Delta = \rho_1 - \rho_2$, $\mu_\Delta = \mu_1 - \mu_2$ and $\epsilon_{ij}^\alpha = \frac{\partial u_i}{\partial x_j} + \frac{\partial u_j}{\partial x_i}$ is the adjoint strain tensor.

The surface integrals arising from the use of the Leibniz integral rule are transformed to volume integrals of $\frac{\delta x_k}{\delta b_n}$, [2], according to $\int_S \Psi R \frac{\delta x_k}{\delta b_n} n_k dS = \int_\Omega \Psi \frac{\partial R}{\partial x_k} \frac{\delta x_k}{\delta b_n} d\Omega$, where $\Psi = \{q, u_i, \psi\}$ denotes every adjoint variable and $R = \left\{R^p, R_i^v, R^\alpha\right\}$ the residual of the corresponding primal problem. By expanding these terms and eliminating the multipliers of $\frac{\delta x_k}{\delta b_n}$, to avoid their computation in the interior of the domain, the adjoint grid displacement PDEs arise, namely

$$\begin{aligned} R_k^{m^\alpha} \;=\; & \frac{\partial^2 m_k^\alpha}{\partial x_j^2} - \frac{\partial}{\partial x_j}\left\{ q \frac{\partial\left(\rho v_j\right)}{\partial x_k} - \rho u_i v_j \frac{\partial v_i}{\partial x_k} - u_j \frac{\partial p}{\partial x_k} + u_i \frac{\partial\left(\mu \epsilon_{ij}\right)}{\partial x_k} - \mu \epsilon_{ij}^\alpha \frac{\partial v_i}{\partial x_k} \right. \\ & \left. - \psi v_j \frac{\partial \alpha}{\partial x_k} - D \frac{\partial \psi}{\partial x_j} \frac{\partial \alpha}{\partial x_k} + D \psi \frac{\partial^2 \alpha}{\partial x_k \partial x_j} \right\} = 0\,, \quad k = 1,2,3 \end{aligned} \tag{20}$$

2.4.2 Adjoint Boundary Conditions

The field adjoint equations are associated with the following boundary conditions:

- Inlets (S_I): Zero Dirichlet and zero Neumann conditions are imposed on ψ and q, respectively. For the normal component of the adjoint velocity $u_{\langle n \rangle} = -\frac{\partial j_{S_{I,i}}}{\partial p} n_i$, whereas the tangential components are set to zero $u_{\langle t \rangle}^I = u_{\langle t \rangle}^{II} = 0$.

- Outlet (S_O): A Robin condition $-\rho_\Delta q v_i n_i - \mu_\Delta u_i \epsilon_{ij} n_j + \psi v_j n_j + D\dfrac{\partial \psi}{\partial x_j} n_j + \dfrac{\partial j_{S_{O,j}}}{\partial \alpha} n_{S_{O,j}} = 0$ is imposed on ψ. Dirichlet conditions of the form $q = u_{\langle n \rangle} v_{\langle n \rangle} + 2\nu \dfrac{\partial u_{\langle n \rangle}}{\partial n} + \dfrac{1}{\rho} \dfrac{\partial j_{S_{O,k}}}{\partial v_i} n_{S_{O,k}} n_i$ and $v_{\langle n \rangle} u_{\langle t \rangle} + \nu \left(\dfrac{\partial u_{\langle t \rangle}}{\partial n} + \dfrac{\partial u_{\langle n \rangle}}{\partial t} \right) + \dfrac{1}{\rho} \dfrac{\partial j_{S_{O,k}}}{\partial v_i} n_{S_{O,k}} t_i = 0$ are imposed on q and u_i, respectively.
- Solid Walls (S_W): A zero Dirichlet boundary condition is imposed on u_i along with zero Neumann conditions on ψ and q.

On the adjoint grid displacement fields m_i^α, a zero Dirichlet condition $m_k^\alpha = 0$ is imposed along all the boundaries of the domain.

2.4.3 Sensitivity Derivatives

After satisfying the adjoint field equations and their boundary conditions, the remaining terms in (the developed form of) eq. 15 stand for the E-SI adjoint SDs, namely

$$\begin{aligned} \left.\frac{\delta J}{\delta b_n}\right|_{E-SI} = & -\int_{S_W} \left[\left(-\rho q n_i + \mu \varepsilon_{ij}^\alpha n_j \right) \frac{\partial v_i}{\partial x_j} n_k + \frac{\partial m_k^\alpha}{\partial x_j} - D\psi \frac{\partial^2 \alpha}{\partial x_k \partial x_j} \right] \frac{\delta x_k}{\delta b_n} n_j dS \\ & + \int_{S_W} D\psi \frac{\partial \alpha}{\partial x_j} \frac{\delta n_j}{\delta b_n} dS \end{aligned} \tag{21}$$

3 On the accuracy of the Sensitivity Derivatives using the Adjoint Formutations

Before proceeding to the application of the proposed method, two studies are carried out to demonstrate (a) the accuracy of the computed derivatives using the adjoint method and (b) the advantages of solving the adjoint to the grid displacement model PDEs accordingly to the E-SI adjoint formulation. In both studies, the flow Reynolds number is $\backsim 350$ and the flow is assumed to be laminar. Also, the properties of the two fluids under consideration remain the same (see table 2) with the diffusion coefficient $D = 1.5 \cdot 10^{-7} m^2/s$. For the purpose of comparison, SDs are computed using both the E-SI and severed E-SI adjoints; in the latter, also abbreviated as SI adjoint, the contribution of the adjoint grid displacement field is omitted from the SDs. Adjoint sensitivities are, also, compared to Finite Differences (FDs).

Firstly, SDs are computed for J_P (eq. 8) in two different 2D geometries/cases. Regarding case 1, a 2D duct with two inlets, from which two different fluids enter the domain, is considered; case 2 pertains to a 2D U-bend duct, the inlet of which is split in half for the two incoming fluids. About 140K and 84K cells, respectively (see fig. 3) were used in each case; both grids are adequately stretched close to the wall in order to resolve the flow boundary layers. B-Splines morphing lattices parameterized the duct's convergent part in case 1 and the duct's U turn in case 2. In fig. 3, the control boxes used in each case are demonstrated. The SDs of J_P w.r.t. the displacements of the active control points in the x and y direction, are computed and plotted in fig. 4. SDs computed based on the E-SI adjoint formulation perfectly match FDs. Exceptionally, in both cases, the SDs based on the SI adjoint (i.e. by omitting the solution of the adjoint grid displacement PDEs) are quite accurate. However, this is a conclusion that cannot be generalized.

Additionally, in case 2, SDs are computed for a different objective function, namely the mean value of α at the exit

$$J_\alpha = \frac{1}{|S_O|} \int_{S_O} \alpha dS \tag{22}$$

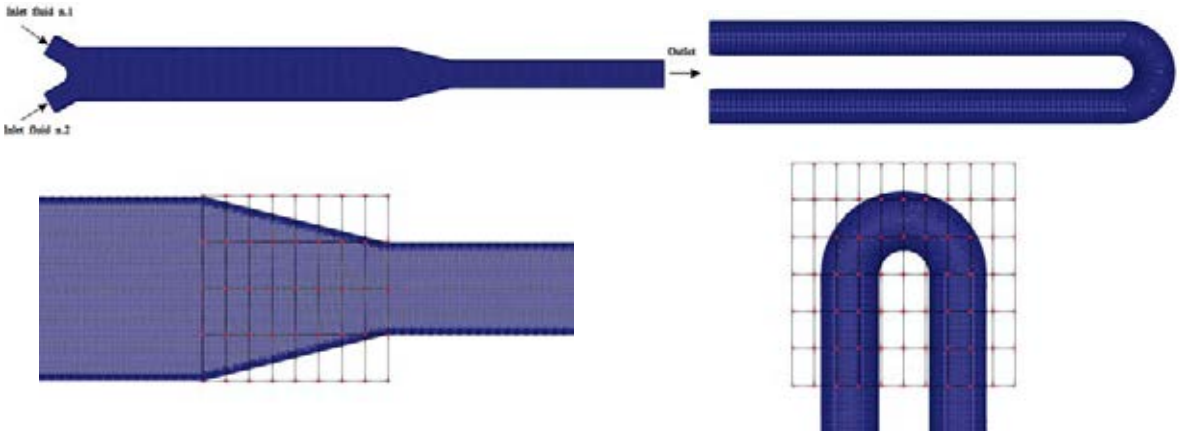

Figure 3: Computational grids and volumetric B-Splines morphing lattices used. Left: Case 1, 2D duct with two inlets. Right: Case 2, U-bend duct. None of these cases includes baffles.

	Fluid 1	Fluid 2
Density (kg/m^3)	1500	1300
Kinematic viscosity (m^2/s)	$1.5 \cdot 10^{-5}$	$1.3 \cdot 10^{-5}$

Table 2: Properties of the two fluids.

The goal of this study is to investigate the accuracy of the computed SDs for a function that depends solely on α and includes surface integrals only at the exit of the domain, similarly to J_U (eq. 7). According to fig. 5, SDs computed based on the E-SI adjoint match almost perfectly those computed with FDs, whereas the severed approach of SI adjoint results in quite wrong SDs for some design variables.

From these studies, the following conclusions can be reached: for the J_P objective, both E-SI and SI adjoints result in the same SDs that also match those computed with FDs, provided that a sufficiently fine grid is used. For the J_α objective, however, SI adjoint may compute inaccurate (or, even, wrongly signed for some design variables) results, as seen in fig. 5. Note that both E-SI and SI adjoints are almost equally fast, since the cost of solving the adjoint grid displacement PDEs (eqs. 20) is negligible compared to the cost of solving the primal and the other adjoint equations.

4 Results

The case geometry is described in section 2.1. Two fluids, with different properties, enter the mixing device, each one from a different inlet. The density and kinematic viscosity of the two fluids are those already presented in table 2. Both fluids have uniform inlet velocity profiles of magnitude $0.1m/s$ at their corresponding inlets; the Reynolds number of the flow, based on the mean value of the viscosity of the two fluids and the duct's inner diameter, is $\backsim 715$ and a laminar flow is assumed. An unstructured hexahedral-based grid consisting of approximately 1.1 M cells is used; the grid is sufficiently refined, especially around the baffles, in order to resolve boundary layers and local recirculations. The flow streamlines, colored by the velocity magnitude, in the reference geometry of the static mixer are shown in fig. 6

The optimization aims at redesigning the shape of each baffle, separately, while the main cylindrical body should remain fixed. Two different approaches for parameterizing the shape of the baffles, namely Node Based Parameterization and Positional Angle Parameterization, are presented in [1]. Herein, a third approach is followed. In specific, each baffle is enclosed by

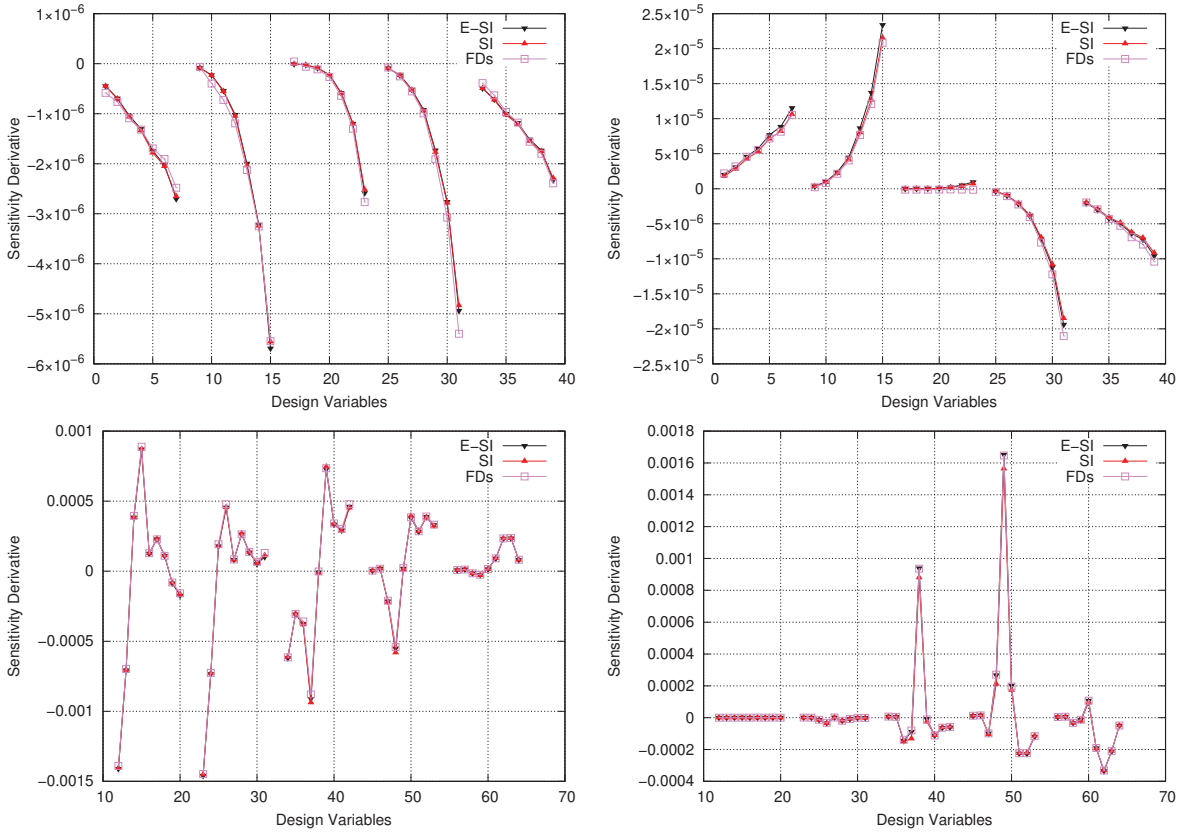

Figure 4: Derivatives of J_P w.r.t. the x (left) and y (right) control points' coordinates, using the SI and E-SI adjoints along with FDs for Case 1 (top) and Case 2 (bottom).

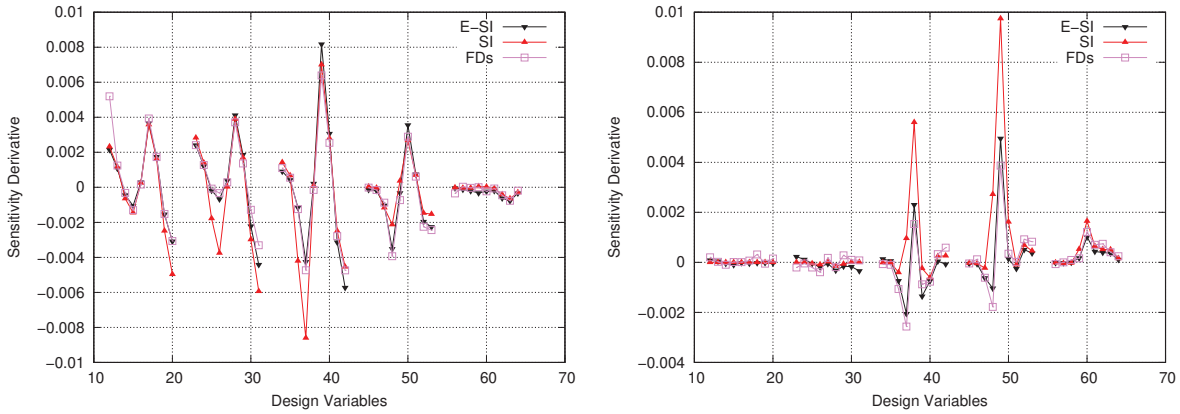

Figure 5: Case 2: derivatives of J_α (eq. 22) w.r.t. the x (left) and y (right) control points' coordinates, using the SI and E-SI adjoints along with FDs.

a single volumetric B-Splines morphing lattice (see fig. 2), which is used to parameterize its shape but, also, the part of the grid residing within its boundaries. The cylindrical coordinates of the control points of the morphing lattices constitute the design variables of the problem. To retain the baffles' thickness for the purpose of manufacturability, the control point coordinates along the axial direction remain fixed. It is important to ensure that grid points existing along the cylindrical body of the duct are not subject to deformations, and that the first row of grid nodes of the baffles remain attached to the circumference of the duct. This issue can easily be addressed by keeping all control points on the outer-most radius of the control lattice fixed.

Figure 6: Stream-lines colored by the velocity magnitude in the reference geometry.

w_1	1	0.5	0.25	0.2	0.1	0
w_2	0	0.5	0.75	0.8	0.9	1

Table 3: Weight combinations used in the objective function J (eq. 10).

The E-SI adjoint formulation (eq. 21) is used to compute the derivatives of the weighted objective function (eq. 10) w.r.t. the coordinates of the control points. For six weight combinations, see table 3, the Pareto front of non-dominated solutions in the two-objective space is computed and plotted in fig. 7; there, the values of J_U and J_P have been divided by the known volume flow rate.

As shown in fig. 7, minimization of total pressure losses and maximization of the mixture's uniformity at the exit are two contradictory targets. For instance, in case with $w_1 = 1, w_2 = 0$, the optimization leads to a huge increase in uniformity (decrease in J_U) by 94% at the exit,

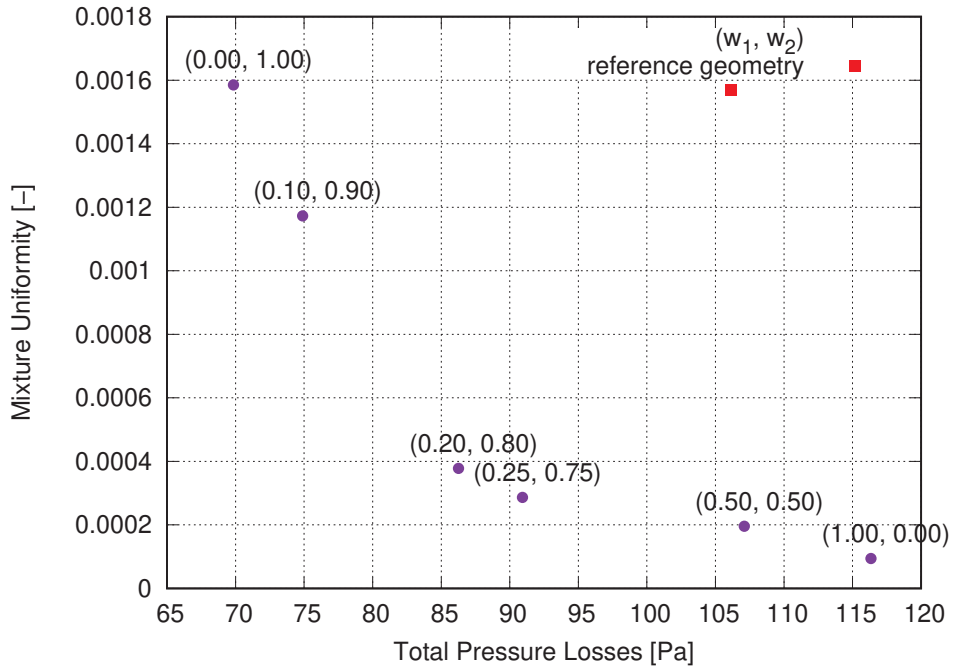

Figure 7: The front of non-dominated optimal solutions in the two objective space computed by the six weight combinations of table 3.

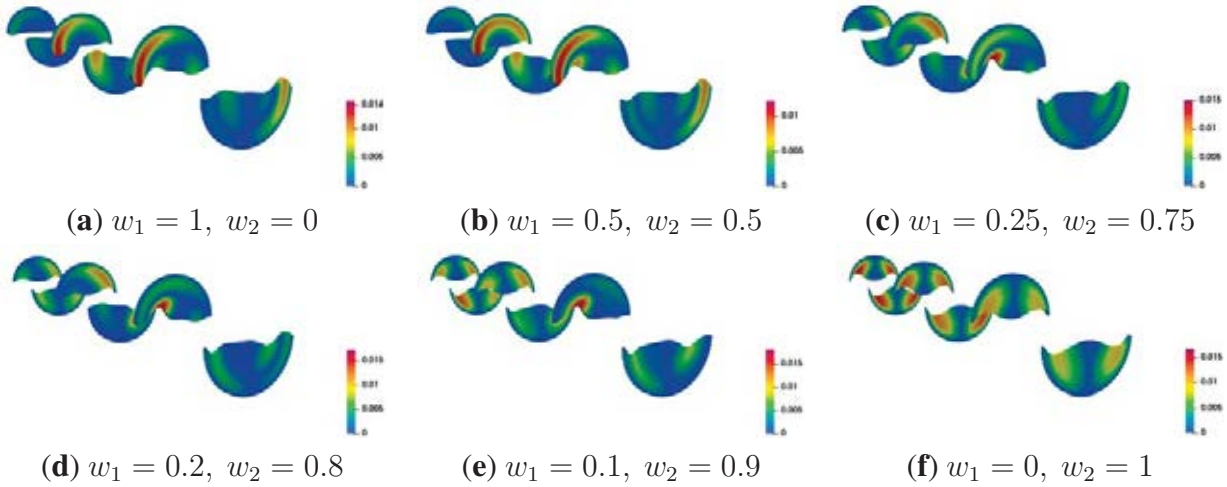

(a) $w_1 = 1,\ w_2 = 0$ **(b)** $w_1 = 0.5,\ w_2 = 0.5$ **(c)** $w_1 = 0.25,\ w_2 = 0.75$

(d) $w_1 = 0.2,\ w_2 = 0.8$ **(e)** $w_1 = 0.1,\ w_2 = 0.9$ **(f)** $w_1 = 0,\ w_2 = 1$

Figure 8: Optimal baffle shapes for each of the six different weight combinations. The baffles are colored by the magnitude of the nodal displacements w.r.t. the reference geometry.

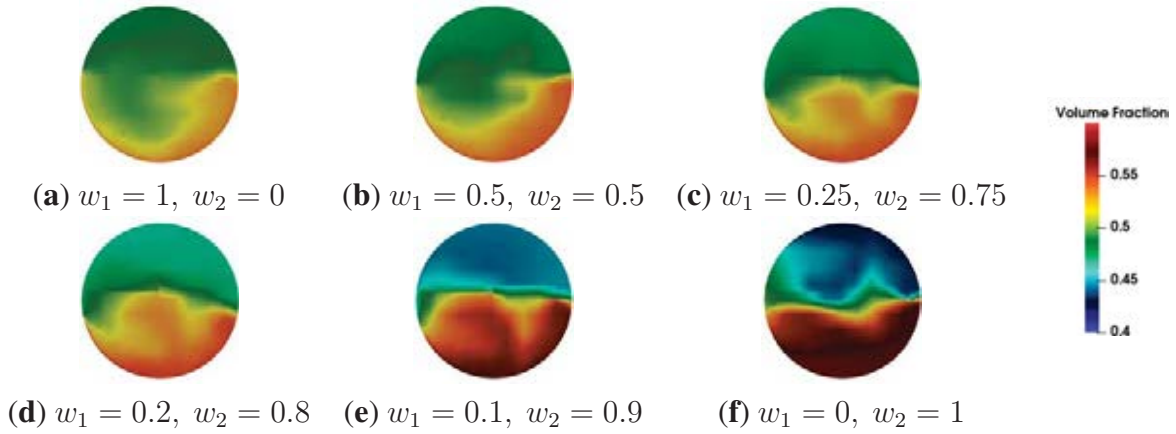

(a) $w_1 = 1,\ w_2 = 0$ **(b)** $w_1 = 0.5,\ w_2 = 0.5$ **(c)** $w_1 = 0.25,\ w_2 = 0.75$

(d) $w_1 = 0.2,\ w_2 = 0.8$ **(e)** $w_1 = 0.1,\ w_2 = 0.9$ **(f)** $w_1 = 0,\ w_2 = 1$

Figure 9: Volume fraction distribution at the exit of the optimized device, for each one of the six weight combinations.

whereas total pressure losses have increased by 9.6% compared to the reference geometry. On the other hand, using $w_1 = 0, w_2 = 1$ leads to a 34% reduction in total pressure losses, at the cost of a slightly lower uniformity at the exit, compared to the reference point.

Fig. 8 shows the final shapes of the six baffles resulting from the optimization for each value-set of weights. By laying emphasis on the minimization of total pressure losses, i.e. working with higher values of w_2, the optimization process leads to the reduction of the baffles cross-sectional area, in order to prevent flow recirculations. Eliminating J_U from the objective function has a negative effect on the mixing effectiveness of the device, see fig. 7.

On the other hand, if priority is given to maximize uniformity at the exit, the optimization tends to create baffles of increased surface and wiggly shape at their tips. By doing so, the vortical structure behind the baffles becomes pronounced helping mixing even more. This is demonstrated in fig. 12 where the tangential component of the velocity is plotted at a cross-section of the static mixer for the reference geometry and the one with the best uniformity. Fig. 9 demonstrates the volume fraction α distribution at the exit for each Pareto point. In addition, figs. 10 and 11 show the flow streamlines colored by the value of volume fraction and total pressure, respectively. In both figures, streamlines are plotted in the reference and optimized geometries corresponding to the two extreme points of the front of non-dominated solutions.

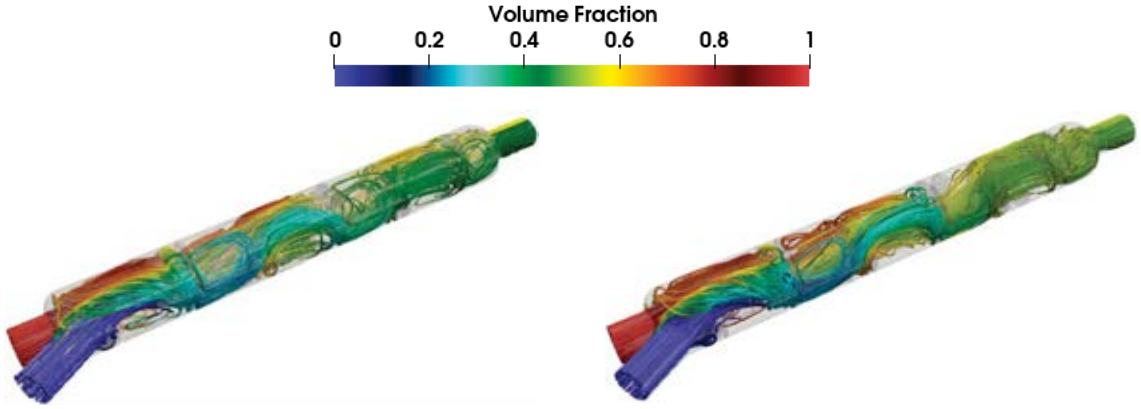

Figure 10: Stream-lines colored by the value of the volume fraction α for the reference (left), and the optimized geometry for min. J_U (right).

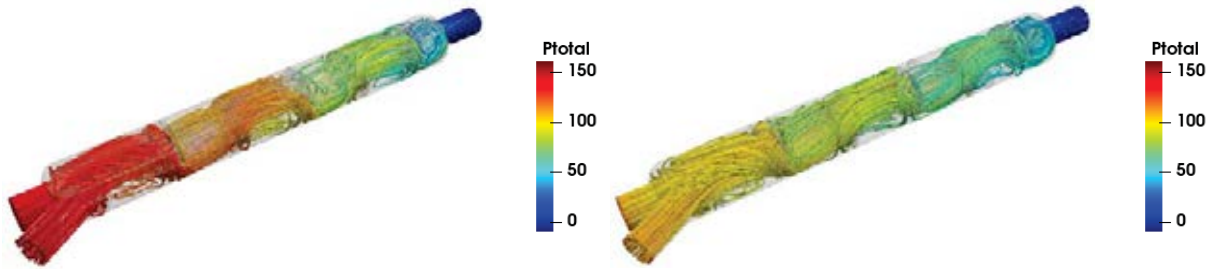

Figure 11: Stream-lines colored by the value of the total pressure for the reference (left), and the optimized geometry for min. J_P (right).

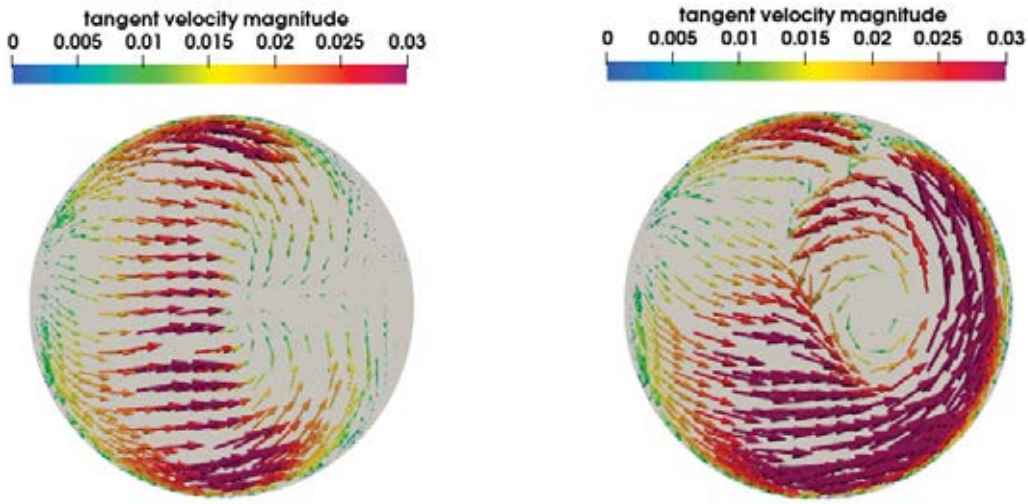

Figure 12: Velocity vectors lying on a cross-section at the middle of the static mixer's length in the reference (left) and optimized for mixture uniformity (right) geometries. In the latter, a highly vortical flow that enhances mixing appears.

5 Conclusions

In this paper, the continuous adjoint method to a two-phase flow model for laminar flows was utilized for the optimization of a mixing device with baffles. Previous works [1], also conducted by the authors' group, where the "severed" adjoint approach was followed, were herein extended, in order to account for the effect of grid sensitivities during the computation

of SDs. The Enhanced-SI (E-SI) adjoint formulation was presented and, then, was used for the optimization of the baffles' shapes by considering two objectives, namely minimization of total pressure losses and maximization of the mixture's uniformity at the exit. First, two studies were conducted in order to assess the accuracy of the computed SDs using the two adjoints, with a reasonable computational cost. There, it was shown that the E-SI and SI adjoints may differ depending on the objective function, with the former computing SDs in good agreement with FDs and the latter occasionally deviating from them.

Regarding the static mixer problem, six optimization runs were performed in total, each of which resulted to optimal baffles of different shapes; the parameterization scheme used, namely a volumetric B-Splines morphing technique, ensured that the baffles' thickness remained fixed during the optimization and their peripheral part remained attached to the body of the mixer. So, the Pareto front of non-dominated solutions in the two-objective space was generated. Each optimal baffle configuration pertains to a single Pareto point; the two extreme points, in specific, indicate two different mechanisms for improving mixing performance and decreasing total pressure losses which are, in fact, contradictory goals. To conclude, a highly uniform mixture at the exit requires wiggly baffles that tend to increase the flow vorticity, whereas decreasing total pressure drop is achieved by creating smaller baffles to minimally disturb the flow.

REFERENCES

[1] P. Alexias, K.C. Giannakoglou, Optimization of a static mixing device with baffles using the continuous adjoint to a two-phase mixing model. *Optimization and Engineering*, **21**, 631–650, 2020.

[2] I.S. Kavvadias, E.M. Papoutsis-Kiachagias, K.C. Giannakoglou, On the proper treatment of grid sensitivities in continuous adjoint methods for shape optimization. *Journal of Comp. Physics*, **301**, 1-18, 2015.

[3] E.M. Papoutsis-Kiachagias, K.C. Giannakoglou, Continuous adjoint methods for turbulent flows, applied to shape and topology optimization: industrial applications. *Archives of Computational Methods in Engineering*, **23**, 255–299, 2016.

[4] K.T. Gkaragkounis, E.M. Papoutsis-Kiachagias, K.C. Giannakoglou, The continuous adjoint method for shape optimization in Conjugate Heat Transfer problems with turbulent incompressible flows. *Applied Thermal Engineering*, **140**, 351–362, 2018.

[5] E.M. Papoutsis-Kiachagias, K.T. Gkaragkounis, A.I. Margetis, T. Skamagkis, V.G. Asouti, K.C. Giannakoglou, *adjointOptimisationFoam*: An OpenFOAM-based framework for adjoint-assisted optimization. *In 14–th ECCOMAS Thematic Conference on Evolutionary and Deterministic Methods for Design, Optimization and Control (EUROGEN 2021)*, Athens, Greece, 17–19 May, 2021.

[6] E.B. Nauman, Enhancement of heat transfer and thermal homogeneity with motionless mixers. *AIChE Journal*, **25**, 246-258, 1979.

[7] H.P. Grace, Dispersion phenomena in high viscosity immiscible fluid systems and application of static mixers as dispersion in such systems. *Chem. Eng. Communications*, **24**, 225–277, 1982.

[8] S.S. Soman, C.M.R. Madhuranthakam, Effects of internal geometry modifications on the dispersive and distrubutive mixing in static mixers. *Chem. Eng. and Processing*, **122**, 31–43, 2017.

[9] H. Song, S.P. Han, A general correlation for pressure drop in kenics static mixer. *Chem. Eng. Science*, **60**, 5696–5704, 2005.

[10] B. Kwon, L. Liebenberg, A.M. Jacobi, W.P. King, Heat transfer enhancement of internal laminar flows using additively manufactured static mixers. *Int. Journal of Heat and Mass Transfer*, **137**, 292–300, 2019.

[11] A. Jameson, Aerodynamic design via control theory. *Journal of Scientific Computing*, **3**, 233–260, 1988.

[12] W.K. Anderson, V. Venkatakrishnan, Aerodynamic design optimization on unstructured grids with a continuous adjoint formulation. *Computers & Fluids*, **28**, 443–480, 1999.

[13] A. Jameson, S. Kim, Reduction of the adjoint gradient formula in the continuous limit. In 41th Aerospace Sci. Meeting and Exhibit, Reno, Nevada, 2003, AIAA 2003–0040.

[14] D.I. Papadimitriou, K.C. Giannakoglou, A continuous adjoint method with objective function derivatives based on boundary integrals for inviscid and viscous flows. *Computers & Fluids*, **36**, 325–341, 2007.

[15] K.T. Gkaragkounis, E.M. Papoutsis-Kiachagias, A.G. Tsolovikos, K.C. Giannakoglou, Effect of Grid Displacement Models on Sensitivity Derivatives computed by the Continuous Adjoint in Aerodynamic and Conjugate Heat Transfer Shape Optimization. *Engineering Optimization*, 2020 (to appear).

[16] C. Brennen, *Fundamentals of multiphase flow*. Cambridge University Press, Cambridge, 2005.

[17] M. Ishii, T. Hibiki, *Thermo-fluid dynamics of two-phase flow*. Springer, New York, USA, 2011.

[18] M.M. Francois, S.J. Cummins, E.D. Dendy, D.B. Kothe, J.M. Sicilian, M.W. Williams, A balanced-force algorithm for continuous and sharp interfacial surface tension models within a volume tracking framework. *Journal of Comp. Physics*, **213**, 141–173, 2006.

[19] S. Popinet, An accurate adaptive solver for surface-tension driven interracial flows. *Journal of Comp. Physics*, **228**, 5838–5866, 2009.